Article:

Birch, CE and Reeder, MJ (2013) Wave-cloud lines over northwest Australia. Quarterly Journal of the Royal Meteorological Society, 139 (674). 1311 - 1326. ISSN 0035-9009

https://doi.org/10.1002/qj.2043

Wave-cloud lines over northwest Australia

Cathryn E. Birch[1] and Michael J. Reeder[2]

For submission to QJRMS

[1]Institute for Climate and Atmospheric Science, School of Earth and Environment, University of Leeds, UK
[2]School of Mathematical Sciences, Monash University, Australia and Centre of Excellence for Climate System Science, Australia

Corresponding author: Cathryn Birch, C.E.Birch@leeds.ac.uk

Keywords: bore, gravity wave, convection, sea breeze, morning glory, heat low

Abstract

The frequency of occurrence and formation mechanisms of wave-cloud lines off the northwest coast of Australia are investigated. Prior to the present study, little was known about these wave-cloud lines. Apart from being spectacular atmospheric phenomenon in their own right, these wave-clouds can have a role in the secondary initiation of convection and can be a hazard to low-flying aircraft. A climatology of wave-clouds, produced from visible satellite imagery, suggests two main types of cloud lines form over northwest Australia. The first are bore-like waves, similar in structure to the "morning glory" of northeast Australia, and occur at least 2-3 times per month throughout the entire year. The second type are convectively-generated cloud lines, which are more circular in shape, appear to originate from convective storms and occur at least 0.5-1.5 times per month during the wet season. High resolution, nested simulations are performed with the Met Office Unified Model for case studies of each type of wave. The bore-like waves occurred in the presence of synoptic-scale, low-level southeasterly flow and a heat low along the northwest coast of Australia. At night, the offshore southeasterlies accelerate into the heat low and collide with the onshore sea breeze. The southeasterlies override the sea breeze and the wave-cloud lines form at the leading edge of this front. The convectively-generated waves radiate outwards from convective storms and produce compensating subsidence for the updrafts in them. These waves take the form of *n*=2 mode wave-fronts, which propagate throughout the entire depth of the troposphere and are similar in structure to waves produced by deep convection that are described in previous studies.

1 Introduction

Large-amplitude internal waves, such as solitary waves and internal bores, commonly occur in the lower atmosphere. They play a role in the initiation and organisation of convection (Koch et al., 2008) and the wind squalls that they produce can be a serious hazard to low-flying aircraft (Christie and Muirhead, 1983). Large-amplitude waves are known to be produced by convection and can propagate along the surface nocturnal inversion layer (Haase and Smith 1984; Koch et al., 2008). Perhaps the most regular and best documented family of large-amplitude waves is the "morning glory" phenomenon, which frequently occurs over the Gulf of Carpentaria in northeast Australia (Clark, 1972; Christie, 1992; Reeder and Smith, 1998). The morning glory is an internal bore, which is often undular and takes the form of a low-level roll cloud, which can extend for more than 100 km. It most commonly develops over the Cape York Peninsula between the months of September and October and propagates from the northeast during the early morning, although it can also form over the land to the south of the Gulf of Carpentaria and propagate from the south (a map of Australia is shown in Figure 1).

The northeasterly morning glory forms through the interaction of two sea breezes, which develop on the west and east side of the Cape York Peninsula (Clarke et al., 1981). The sea breezes develop during the day and penetrate inland until they converge. The easterly geostrophic wind limits the strength of the west-coast sea breeze and, therefore, at the point of collision the west-coast sea breeze is shallower and more stable than the east-coast breeze. The east-coast sea breeze overrides the west-coast breeze, which causes a disturbance that can produce waves that propagate along the surface-based stable layer formed by the west-coast sea breeze (Goler and Reeder, 2003). Depending on the stability and depth of the stable layer, the waves can amplify and propagate along the stable layer at speeds that are much greater than the propagation speed of the east-coast sea breeze (Thomsen et al., 2009; Reeder et al., 2012).

The southerly morning glory develops over the land to the south of the Gulf of Carpentaria and propagates northwards. It forms when cold fronts propagate northwards over central Australia and merge with the heat trough that is present over northern Australia during the warmer months (Smith et al., 1995). The fronts are relatively weak during the day due to strong turbulent mixing but after sunset the mixing subsides and the ageostrophic wind component increases, which intensifies the front (Deslandes et al., 1995). In the early morning bore-like waves can form at the leading edge of the front, which propagate ahead of the frontal zone on a pre-existing low-level nocturnal inversion layer. Schmidt and Goler (2010) also describe the formation of nonlinear waves and cloud-lines ahead of cold fronts over the ocean. They show that when cold fronts in the Great Australian Bight (to the south of the Australian continent) advance into a marine inversion, wave clouds can form at the leading edge of the cold air mass.

Wave-cloud lines over northwest Australia have not been studied in detail (Christie, 1992). Neal and Butterworth (1973) and Clarke (1981) present satellite imagery of cloud lines over northwest Australia, which are many 100's km long, similar in structure to the morning glory and propagate northwestwards, far out over the Indian Ocean. Kingwell (1984) also identified a cloud-line off the northwest coast, which appeared to originate near Broome, to the north of an intense thunderstorm. The wave expanded radially over the sea, in a quasi-circular arc and appeared to have been triggered by a density current associated with the region of deep convection.

Smith (1986) presents the only detailed study of wave-cloud lines over northwest Australia. Two spectacular low-level cloud lines, similar to the morning glory, were observed and photographed from a ship to the northwest of Port Hedland at 2000 and 2030 Western Australian Time (WST), 10th November 1983. The cloud lines were orientated approximately west-east and propagated towards the north for at least 18 hours, at speeds of approximately 10 m s^{-1}. A region of thunderstorms were present over the land to the south of Port Hedland during the afternoon of 10th November. Smith (1986) suggests that the cloud lines were bore-like disturbances, generated by the interaction between the onshore sea breeze and a northward-propagating gust front that was produced by the convective storms. Radiosonde observations from Port Hedland at 0700 WST, 10th November 1986 show a stable layer adjacent to the surface, which was formed by the previous day's sea breeze and diurnally-driven surface radiative cooling, and a near-neutral layer above, which was formed by strong diurnal heating on the previous day. Smith (1986) suggests that the stable layer, capped by the near-neutral layer could have acted as an effective waveguide for the propagation of disturbances produced by the collision of the two flows.

Bretherton and Smolarkiewicz (1989) show that convective clouds can produce tropospheric gravity waves that propagate radially away from the system, providing compensating subsidence and adiabatic warming outside the convective cloud. Mapes (1993) applied this idea to mesoscale convective systems in the tropics; he suggested that large convective systems can generate horizontally propagating bores, which have vertical wavelengths that are harmonics of the depth of troposphere. The n=1 wave mode has a vertical wavelength equal to twice the depth of the troposphere; it travels fast and induces deep subsidence. The n=2 mode has a vertical wavelength equal to the depth of the troposphere; it travels slower than the n=1 mode and can either induce ascent in the lower troposphere and descent in the upper troposphere (Mapes, 1993), or descent in the lower troposphere and ascent in the upper troposphere (Marsham and Parker, 2006). If the n=2 wave mode causes air to be displaced upwards, above its lifting condensation level, wave clouds will form. Wave-induced upward displacement of air in the lower troposphere can also initiate new convective cells if air close to the surface is lifted above its level of free convection (e.g. Lane and Reeder, 2001; Lac et al., 2002; Birch et al., 2012).

This paper studies the occurrence and formation mechanisms of wave-cloud lines that are generated near the northwest coast of Australia. Section 2 introduces examples of the types of waves that occur over the region and presents a satellite-derived monthly climatology of wave-cloud occurrence. Section 3 describes the model set-up and the simulations that were performed. Section 4 presents the results from the first (bore-like wave) model case study and describes the mechanisms for the development and propagation of the waves. Section 5 presents the results from the second (convectively-generated wave) model case study, and the discussion and conclusions are presented in section 6.

2 Observed wave types and frequency of occurrence

Figure 2 shows visible satellite imagery from the Multi-Functional Transport Satellite (MTSAT) at (a) 1100 Western Australian Time (WST), 22nd November 2011, (b) 0800 WST, 23rd November 2011 and (c) 1100 WST, 31st January 2011. Figure 2a shows a series of linear cloud lines over the sea, approximately 500 km off the northwest coast of Australia (W1) and a second cloud line that is much closer to the coast (W2). It is known that these cloud lines were relatively low because they are not apparent in the infra-red satellite imagery. Similar cloud lines were observed on the following day (Figure 2b); the main cloud lines span almost 1000 km from Exmouth in the southwest corner of the image, to north of Broome (W3 and W4, see Figure 1 for locations of places mentioned in the text). An additional cloud line is also visible in this image, approximately 400 km to the west of Darwin. The waves on both days propagate towards the northwest and since there is little or no convection to the southeast of these cloud lines, it seems unlikely that they were produced by convective storms. These clouds appear to be bore-like waves, similar to the morning glory, which occurs regularly in northeast Australia between September and mid-November.

Figure 2c shows two additional low-level wave clouds in northwestern Australia. In contrast to the examples described above, these clouds are more concentric in shape and appear to be emitted from the two convective storms over the coast. The cloud line associated with the first region of convection (C1) propagates towards the north and the cloud line associated with the second region of convection (C2) propagates towards the west.

All visible satellite images available from MTSAT between 2006-2011 were examined to generate a climatology of wave-cloud lines over northwestern Australia. Wave clouds, such as those illustrated in Figure 2, were identified and the date and wave-cloud type were recorded (bore-like or convectively generated). Differentiation between the types of cloud lines was subjective; convective wave clouds appeared more concentric in shape, originated from regions of deep convection and propagated in any direction, whereas bore-like wave clouds appeared more linear and always propagated away from the coast. The monthly average number of wave-cloud lines identified per year during the six year period is shown in Figure 3. Bore-like wave clouds were identified during all months of the year, although fewer were identified between January and March. The wet season occurs during these months (Drosdowsky, 1996), which suggests that either the increased number of convective systems prevent these clouds from forming, or that the deep convective cloud masks the wave-cloud lines in the satellite imagery. Most of the waves were identified in the 0800 and 1100 WST satellite images, although many persisted until 1400 or 1700 WST. Wave clouds that appeared to originate from convective storms were only identified during the wet season (December-April), because most convective systems that develop over northwestern Australia occur during these months (Pope et al., 2008).

Outside of the wet season, 2-3 bore-like wave clouds were identified on average per month in a given year and 0.3-1.5 convectively-generated wave clouds were identified on average per month in a given year during the wet season. This is likely to be fewer than actually occurred because: (a) the satellite spatial and temporal resolution may not have been high enough to identify all the cloud lines, (b) only clouds that occurred during daylight hours could be identified because the clouds do not appear in the infra-red satellite imagery, (c) high cloud may mask the low-level cloud lines in the satellite imagery and (d) waves may have been generated that did not produce cloud and thus would not appear in the satellite imagery.

The wave clouds illustrated in Figure 2 are good examples of the bore-like and convectively-generated waves that were identified during the generation of the cloud-line climatology. Model simulations of the two cases are now used to investigate the initiation mechanisms, the wave structure and the synoptic-scale weather situations associated with the development of these waves.

3 Model simulations

The two case studies were simulated using version 7.3 (Parallel Suite 22) of the Met Office Unified Model (MetUM). The MetUM has a semi-Lagrangian, semi-implicit and non-hydrostatic formulation and a terrain-following co-ordinate system (Davies et al., 2005). Many types of process are parameterised, such as the surface (Essery et al., 2001), the boundary layer (Lock et al., 2000) and mixed-phase cloud microphysics (Wilson and Ballard, 1999). Convection is parameterised in the global and 12-km nest using the Gregory and Rowntree (1990) scheme. For the 4-km simulations with explicit convection, the convection parameterisation scheme is effectively switched off.

The first case study includes the overnight development of wave-cloud lines on both 21st-22nd and 22nd-23rd November 2011. To capture both these events the model was initialised at 0000 UTC (0800 WST), 21st November 2011 and run for 60 hours. The focus of the second case study is convectively-generated wave-cloud lines, which occurred around 1100 WST, 31st January 2011. For this case the model was initialised 0000 UTC (0800 WST), 30th January 2011 and run for 48 hours. For both case studies the global model was initialised using an operational MetUM analysis and was used to create lateral boundary conditions for the 12-km resolution nest. The 12-km nest then created lateral boundary conditions and initial conditions for the 4-km resolution nest. The limits of the 12 and 4-km model domains are illustrated in Figure 1.

4 Case study one: Bore-like waves

4.1 Synoptic situation and wave overview

Figure 4 shows 925 hPa virtual potential temperature, θ_v, 925 hPa wind vectors and mean sea level pressure (MSLP) at three times during the model simulation that was performed for the first case study. Throughout the period a region of high pressure persists over southern Australia and heat low centres exist over northern Australia; at 1500 WST, 21st November 2011 there are two main heat low centres at 128ºE, 19ºS and 143ºE, 25ºS (Figure 4a) . The heat low to the west extends along the northwest coast towards Exmouth. There is cyclonic (i.e. clockwise in the southern hemisphere) circulation around the heat low and southeasterly flow to the south of it, which is forced by the high pressure centre over southern Australia. This southeasterly flow produces a strong offshore breeze between Exmouth and Broome, which converges with an onshore flow during the afternoon of the 21st November. This onshore flow is a sea breeze circulation, formed due to the daytime temperature difference between the land and sea (e.g. Davis et al., 1889; Atkinson, 1981) and appears to be reinforced by the northwesterly and westerly winds associated with the northern part of the cyclonic circulation around the heat low.

The two heat low centres weaken overnight and by 0100 WST, 22nd November the westward extension of the heat low has formed a separate heat low centre at 115ºE, 21ºS (Figure 4b). Cyclonic circulation around all three heat low centres is apparent at this time and due to the decreased effects of turbulence overnight, the offshore southeasterly winds are stronger than during the day. This is shown more clearly in plots of the ageostrophic wind component. During the evening and overnight the 925 hPa ageostrophic wind speeds are high and the flow is directed into the heat low and off the northwest coast (Figure 5a). During the morning and early afternoon the heat low is less developed and the impact of turbulence higher, and thus the ageostrophic wind component is much weaker (Figure 5b). This diurnal variation in the ageostrophic wind is examined in detail by Arnup and Reeder (2007).

The synoptic-scale situation and diurnal variations during the second part of the case study are similar to that in the first. The high pressure persists to the south and the heat low to the south of Darwin (see Figure 1 for location) deepens during the day (not shown). By 0100 WST, 23rd November there is strong southeasterly offshore flow along the northwest coast (Figure 4c). The main difference between 0100 WST on the 22nd and 23rd November is that the secondary heat low to the west has moved southwards, down the west coast from 115ºE, 21ºS to 114ºE, 25ºS. The result of this is that the onshore sea breeze during the second half of the case study is weaker than during the first.

The propagation of the bore-like waves is best illustrated using plots of 925 hPa vertical velocity (Figure 6). On the afternoon of the 21st November the extent of the onshore sea breeze is marked by the red band of upward vertical velocity that extends from Exmouth to 123ºE, 20ºS (Figure 6a). The wind vectors show that this is where the southeasterly winds associated with the high pressure system to the south converge with the southwesterly or westerly onshore winds associated with the sea breeze and the cyclonic circulation round the heat low. Over the course of the afternoon, as the sea breeze intensifies, this convergence line moves inland from the coast (Figure 6b). There is another west-east band of upward vertical velocity immediately to the south of the first, which extends from 121.5ºE, 21.5ºS and 123.5ºE, 21.5ºS. This band propagates northwards during the afternoon and reaches the first convergence line at approximately 1700 WST. Following this, a band of upward vertical velocity begins to move northwestwards, crossing the coast between 2100 and 2200 WST (Figures 6c and d). The band marks the leading edge of the southeasterly flow, which advances towards the northwest overnight and produces the cloud that is associated with the first wave (W1). At approximately 0600 WST a second wave forms off the coast and also propagates towards the northwest (W2, Figure 6f).

A similar mechanism appears to generate the waves that occur on the second day of the case study. The convergence zone develops along the northwest coast (Figure 6g), although this time it does not propagate as far inland because the onshore winds are weaker. At 2000 WST, 22nd November the band of upwards vertical velocity moves out, over the coast and forms two waves (W3 and W4), with similar structures to those on the previous day (Figure 6h).

4.2 Wave formation and propagation

Figure 7 shows θ_v and wind vectors along the diagonal transect marked by the black line in Figures 4 to 6. The convergence zone formed by the confluence of the southeasterly offshore winds with the onshore sea breeze is marked by the region of higher temperatures at 20.5ºS in Figure 7a. This zone also coincides with a region of large, positive sensible heat fluxes, low humidity and high temperatures, caused by a region of very dry soil close to the coast (20-21ºS, Figure 8). Inland of the convergence zone the boundary layer is reasonably warm and extends to approximately 1700 m above mean sea level. In contrast, to the northwest over the sea the boundary layer is only 350-700 m deep and is much cooler. Both boundary layers are capped by a temperature inversion, which is approximately 400 m deep over land but more than 1 km deep over the sea. Qian et al. (2012) show through an idealised modelling study that the presence of a moderately-steep plateau, inland of the coast, can block the inland propagation of the sea-breeze and strengthen the off-shore flow. It is possible that the relatively gradual increase in orography height, from zero at the coast to 280 m 150 km inland of the coast (Figure 8a), has a similar effect here.

By 1800 WST the offshore southeasterly winds have intensified and undulations in the inversion above the marine boundary layer start to develop at 19.2ºS (Figure 7b). W1 becomes visible in the θ_v section at 2300 WST (Figure 7c); it occurs at the leading edge of the front formed by the southeasterly winds, which begin to override the sea breeze. The overriding of the sea breeze is shown clearly in contour plots of horizontal (along transect) winds (Figure 9). Figure 9a shows the collision of the offshore southeasterly flow with the onshore sea breeze at low levels (blue and red shading below 1.5 km). By 2200 WST the southeasterly flow has intensified and begins to override the low-level sea breeze (Figure 9b). The wave forms at the leading edge of the southeasterly flow, which is at approximately 18.6 and 17.5ºS at 0200 and 0700 WST respectively (W1, Figure 9c and d).

The second wave on the first day (W2) forms in the early hours of the 22nd November. At this time the sea breeze is very weak and the offshore southeasterlies are at a maximum (Figure 9d). The offshore winds push the sea breeze backwards, over the sea to 18.7ºS at 1000 WST, 22nd November. The collision and convergence of the two flows causes upward motion, which is illustrated by the θ_v contours between 1 and 2.5 km at 18.7ºS in Figure 7e. This wave also propagates towards the northwest.

The mechanism for the formation of the first wave on the second day (W3) is similar to that for the first wave on the first day (W1). The convergence zone develops during the day at 20ºS (Figure 7f), except it is closer to the coast than on the first day because the onshore sea breeze is weaker and the offshore flow stronger (compare Figure 9f with 9a). During the evening the southeasterly offshore wind intensifies and beings to override the sea breeze (Figure 9f and g). The leading edge of the overriding southeasterly air forms the wave, which propagates towards the northwest (Figure 7g and h). The southeasterly winds push further out over the coast on the second day because the counteracting onshore sea breeze is weaker on this day (compare Figure 9h and c).

The second wave on the second day (W4) forms in the same way as W2, although the details are slightly different. The convergence of low-level onshore and offshore flows creates a wave-like structure, with a region of ascent leading a region of descent (marked W4 in Figures 7h and 9h). The offshore southeasterlies are stronger and the sea breeze is weaker on the second day, which means the low-level southeasterly surge occurs earlier in the evening and thus, compared with W1 and W2, W3 and W4 are closer together in space and time.

An overview of the propagation of the waves is best illustrated using a Hovmöller plot of the vertical velocity at 2000 m above mean sea level (Figure 10). The black dashed line marks the location of the coastline in the diagonal section. The regions of intense upward vertical velocity at 20.5ºS on the 21st November and 19.7ºS on the 22nd November clearly show that the convergence zone was further inland on the first day. The solid black lines in Figure 10 mark the propagation of the four waves. The upward motion associated with the two main waves (W1 and W3) are very distinct in the vertical velocity plots at this altitude, whereas it is less so for W2 and W4.

Hovmöller plots of along-transect wind speed at 200 m and 2000 m above ground level give a good overview of the formation mechanisms and propagation of all four waves (Figure 11). During the first day of the case study (21st November) the onshore sea breeze develops during the daytime (blue colours) and converges with the offshore southeasterly flow (red colours) at 20.5ºS. After sunset, at approximately 1900 WST, the sea breeze weakens and the offshore southeasterly flow intensifies and pushes outwards over the sea. The leading edge of the southeasterly flow overrides the sea breeze and forms the first wave (W1). The overriding of the sea breeze is illustrated in Figure 11 by the fact that the winds immediately behind the front (W1) are stronger at 1000 m compared to at 200 m (20-17ºS, 1800 WST 21st November to 0600 WST 22nd November). W2 has a larger effect on the near-surface winds than W1 (Figure 11a). W2 occurs later in the evening when, due to reduced turbulent mixing, the southeasterly offshore flow is at its maximum. At this time the offshore flow is able to completely overcome the onshore sea breeze at low levels, which produces a second surge in the southeasterly offshore flow close to the surface.

On the second day of the case study (22nd November) the sea breeze is weaker and the southeasterlies are stronger (Figure 11a). Similar to the first day/night, the sea breeze weakens in the evening and the offshore southeasterly winds intensify, which causes the offshore flow to override the sea breeze (W3). The second surge is not as intense in this case because the strong southeasterly winds were able to push back the weak onshore sea breeze in the first surge. Propagation speeds of the waves can be computed from the Hovmöller plots: W1 propagates with a speed of 11.1 m s^{-1}, W2 with a speed of 5.7 m s^{-1}, W3 with a speed of 12.2 m s^{-1} and W4 with a speed of 9.3 m s^{-1}.

Figure 12 shows vertical velocity, θ_v and total cloud water content along the diagonal line transect. The times chosen best illustrate the cloud associated with each of the four waves. On the first day/night of the case study (21st-22nd November) a region of cloud forms over the land between 24 and 21ºS (Figure 12a). W1 and W2 are visible in the θ_v contours and there is cloud associated with both of them between 750 and 1200 m. It is this cloud that is visible in the satellite imagery in Figure 2a. Cloud is also associated with the waves on the second day of the case study (Figure 12b); in the model most of the cloud is associated with the second wave (W4) in this case, whereas in the satellite imagery (Figure 1b) both waves appear to produce cloud.

The formation mechanisms of the waves are summarised in Figure 13. During the day the offshore flow is deep and warm but the wind speeds are relatively weak. The onshore sea breeze is cool, shallow, capped by an inversion and the wind speeds are relatively strong. The two opposing flows converge just inland of the coast (Figure 13a). After sunset the offshore winds accelerate and the sea breeze weakens. The offshore flow advances forward and begins to override the onshore sea breeze. The first wave forms at the leading edge of the advancing offshore flow and disturbances begin to form on the inversion layer that caps the sea breeze (Figure 13b). By the next morning the onshore sea breeze has almost completely subsided but the offshore flow is still strong. At this point the low-level offshore flow is able to overcome the sea breeze and push it backwards. The second wave forms at the leading edge of this (Figure 13c).

Zhang and Koch (2000), Koch et al. (2001), Thomsen et al. (2009), Schmidt and Goler (2010) and Reeder et al. (2012) describe cases in which wave disturbances are formed by the collision of a density current (i.e. a cold front or sea breeze) and a surface-based inversion layer. After the collision, the density current begins to override the inversion layer and waves can form at its leading edge. The speed of the fastest mode of bore-like waves that is able to propagate along the inversion, c_0, was be computed following Haase and Smith (1984):

$$c_0 = u + \mathrm{c} \qquad (1)$$

where c is the theoretical wave phase speed in the inversion layer and u is the horizontal wind speed in the inversion layer. c_f is the propagation speed of the leading edge of the density current or front (Figure 13b illustrates u and c_f). If $c_f < c_0$ the flow is said to be subcritical; i.e. the inversion layer is sufficiently deep and stable to support waves that propagate faster than the propagation speed of the front. When these conditions occur the wave disturbance propagates ahead of the front and can evolve into large-amplitude solitary waves. If $c_f > c_0$ the flow is said to be supercritical; i.e. the inversion layer is not sufficiently deep or stable to support waves that can propagate ahead of the front. In this case the leading edge of the front becomes wave-like but the waves remain attached to the front.

The cases presented in this study are different to those described previously; here the inversion is elevated above a well-mixed marine boundary layer, as opposed to adjacent to the surface as in the previous cases. The derivation presented in the Appendix is an extension of that by Scorer (1997) and shows that for cases with an elevated inversion layer, the solution is different. Equation A2 can be solved numerically for c if N_2 (Brunt-Väisäla frequency of the inversion layer ahead of the density current), N_3 (Brunt-Väisäla frequency of the near-neutral layer above the inversion), H (depth of well-mixed marine boundary layer) and h (depth of the elevated inversion layer) are known (see Figure 13b). The values of u, N_2, N_3, H and h and the likely errors associated with their graphical estimation are determined from Figures 7 and 9 and plots of the Brunt-Väisäla frequency (not shown) for both days of the case study.

On the first day of the simulation (W1), u = -1.0±1.0 m s^{-1}, N_2 = 0.0175±0.001 s^{-1}, N_3 = 0.0100±0.001 s^{-1}, H = 600±100 m and h = 400±100 m, and therefore c = 6.5±1.2 m s^{-1} and c_0 = 5.5±2.2 m s^{-1}. c_f is determined from the Hovmöller plot in Figure 10 and is equal to 11.1±0.5 m s^{-1}. Even when the large uncertainty associated with graphical estimation is taken into account, $c_f > c_0$ and the flow is, therefore, supercritical. The leading edge of the offshore flow can become wave-like, but waves cannot propagate ahead of the advancing front in the elevated inversion layer. On the second day of the simulation (W3), c_f = 12.2 m s^{-1}, u = 2.0±1.0 m s^{-1}, N_2 = 0.0145±0.001 s^{-1}, N_3 = 0.007±0.001 s^{-1}, H = 750±100 m and h = 700±100 m, and therefore c = 8.9±1.4 m s^{-1} and c_0 = 10.9±2.4 m s^{-1}. In this case $c_f > c_0$ but the difference is smaller than on the first day, which means that although the flow is supercritical, it is near the supercritical-subcritical transition point.

4.3 Favourable conditions for wave formation

The wave formation mechanism described above has been demonstrated using model simulations of wave occurrences on two consecutive days. Favourable synoptic conditions appear to include a high pressure region over southern Australia that causes low-level southeasterly offshore winds along the northwest coast, an onshore sea breeze during the day and early evening and a perhaps of secondary importance, a heat low along the northwest Australian coast. During the evening and overnight the winds accelerate into the heat low and collide with the onshore sea breeze, which forms the cloud lines that propagate towards the northwest.

MSLP and 950 hPa horizontal winds from ERA-Interim (Dee et al., 2011) can be used to compare the synoptic-scale circulation on days when bore-like wave clouds were identified in the satellite imagery with climatology. Figure 13a shows MSLP and 950 hPa wind vectors at 1800 UTC (0200 WST), averaged over 2006-2011. On average there is a region of high pressure over southern Australia and along the northwest coast of Australia the winds are northerly or northwesterly. Figure 13b shows the same ERA-Interim diagnostics but averaged only over days when a bore-like wave-cloud was identified. On these days the high pressure region over southern Australia is stronger than in the climatology and thus the pressure gradient between southern Australia and the northwest coast is greater. For this reason the 950 hPa winds are stronger and are southeasterly, as opposed to the northerly or northwesterly winds in the climatology.

5 Case study two: Waves from convective storms

The second type of wave identified from the satellite imagery appeared to be convectively generated. One of the best examples of this type of wave was identified from the satellite imagery at 0800 WST, 31st January 2011 (Figure 2c). This day forms the second case study, in which model simulations are used to document the origin and structure of the waves.

Figure 2c shows three main regions of convection, two near the coast (labelled C1 and C2) and one farther inland (labelled C3). Figure 14 shows model vertical velocity at 0800 and 0930 WST, 31st January 2011. The model reproduces the region of convection that spans the coast from 120 to 130ºE (C1) and the region of inland convection (C3), but the convection to the south of Darwin (C2) is not apparent in the model diagnostics. Waves, identified by bands of upward and downward vertical velocity, are emitted from the model convective clouds during the morning of 31st January 2011. This structure is illustrated most clearly in the northeast part of C1 (at 128ºE, 15.5ºS) in the model, where the circular bands of up and downward vertical velocity propagate away from the centre of the convective cell. The waves associated with this cell are analysed in the remainder of this section.

Cross sections of vertical velocity, wind speed and θ_v along a 128ºE transect are shown in Figure 15. The centre of the storm is immediately inland of the coast (14.8ºS) and is marked by a region of strong downward vertical velocity that extends to more than 8 km above mean sea level. In the lowest 2 km there is offshore flow over the land (18-14.5ºS) and onshore flow over the sea (14.5-12ºS), which is likely related to a sea breeze circulation. Above 2 km the winds are southeasterly along the whole diagonal transect. This wind structure is also illustrated by the 850 and 600 hPa wind vectors in Figure 14a and b respectively. A pool of cold air, produced by evaporation, is adjacent to the surface between 15.8 and 14.8ºS. Hovmöller plots at 200 m above ground level (not shown) suggest that the pool of cold air does not propagate horizontally and does not generate the waves.

The waves that are illustrated by concentric bands of 850 hPa vertical velocity in Figure 14 can be identified in the vertical sections by the regions of strong upward and downward vertical velocity below 4 km. The locations of the waves to the north and south of the storm are labelled (convective storm wave) CSW1a and CSW1b respectively. CSW1a causes downward displacement of air below 4 km and upward displacement of air between 4.5 and 6 km (Figure 15). Conversely, CSW1b causes upward displacement of air below 4 km and downward displacement of air between 5 and 7 km. Both waves appear to be mode *n*=2 (i.e. one vertical wavelength) wave-front type waves, that propagate throughout the depth of the troposphere, rather than an undular bore or advecting front as discussed in section 4. Previous studies (e.g. Mapes, 1993; Lane and Reeder, 2001; Marsham and Parker, 2006; Lane and Zhang, 2011; Birch et al., 2012;) have shown that the *n*=2 wave mode can produce either upward or downward displacement of air in the lower atmosphere, which is related to the shape of the vertical profile of diabatic heating (Mapes, 1993).

Neither of the convectively-generated waves produce any cloud in the model. This could be because the *n*=2 model wave, that propagated over the sea, towards the northwest (CSW1a), produced downward rather than upward displacement of air in the lowest 4 km. Without lifting air above its condensation level, cloud will not form. It could be that if the model had produced upward displacement of air in the CSW1a wave, cloud would have been produced in the model. Upward displacement of air does however, occur in the lower atmosphere in CSW1b; cloud is probably not formed in this wave because it is propagating inland, through warmer, less humid air, which is not displaced above its condensation level by the wave.

The propagation of the two convectively-generated waves is illustrated in the Hovmöller plot of 850 hPa vertical velocity along 128ºE (Figure 16). The convective cloud fraction model diagnostic is also illustrated by the thick white contour. The convective storm is reasonably stationary between 0600 and 1400 WST, 31st January and is located just inland of the coast, between 14.5 and 15.7ºS. Between 0700 and 0800 WST, during a period of significant updrafts in the convective storm, CSW1a and CSW1b are emitted from the convective system during the updrafts and propagate towards the north and the south at speeds of 15.1 and 9.8 m s^{-1} respectively (thick black lines in Figure 16). The wave that propagates to the south is slower because it is propagating into the large-scale flow. Note that the *n*=1 and *n*=3 wave modes are not apparent in the Hovmöller plot.

6 Discussion and conclusions

Prior to this study, the frequency of wave-cloud occurrences over northwest Australia, their structure and their formation mechanisms were unknown. This study has shown that two main types of wave-cloud lines occur: (a) bore-like wave clouds, similar to the morning glory, which were identified in the 2006-2011 satellite imagery at least 2-3 times per month and (b) convectively-generated wave clouds, which were identified 0.3-1.5 times per month, but only during the wet season (December-April).

Good examples of both types of wave were identified from the satellite imagery and nested high-resolution simulations were performed for each case with the Met Office Unified Model (MetUM). Bore-like wave clouds occurred on two consecutive days during the first case study. During this period a ridge of high pressure was present over South Australia, there were southeasterly low-level winds over northwest Australia and a heat low spanned the northwest coast. An onshore sea breeze was present on both days of the case studies, which formed due to the difference in daytime surface temperature between the land and sea. On the first day of the case study, the onshore sea breeze was reinforced by the cyclonic (clockwise) circulation around the heat low. As turbulent mixing decreased in the evening and overnight, the winds accelerated into the heat low, which increased the speed of the offshore southeasterly flow. The offshore flow collided with shallower onshore sea breeze and began to override it.

Computations following Haase and Smith (1989) and Scorer (1997) suggest that the collision was supercritical, i.e. that the elevated stable layer associated with the sea breeze was not deep or stable enough to allow waves to propagate along the inversion at speeds greater than the advancing southeasterly flow. For this reason the waves were not strictly bores but were formed in the leading edge of the offshore southeasterly flow. A second wave also formed several hours later on both days of the case study. This was caused by a later surge in the near-surface southeasterly flow, which pushed the sea breeze back over the sea.

The formation mechanism for the first wave on both days of the case study appears to be similar to the formation mechanism of the nonlinear waves that form ahead of cold fronts in the Great Australian Bight (Schmidt and Goler, 2010). In both cases a propagating air mass collides supercritically with an inversion layer, overrides it and forms waves at its leading edge. An important distinction between the cases described in this study and the wave disturbances that form in both the Great Australian Bight and northeast Australia is that the latter involve a surface-based inversion, whereas in the former case the inversion is elevated.

A comparison was made between an ERA-Interim climatology of 950 hPa winds and MSLP at 0200 WST with the same diagnostics but averaged only over days when a bore-like wave was identified in the satellite imagery. The comparison shows that on days when a bore-like wave formed, higher than average pressure occurs over South Australia and the synoptic-scale low-level winds are southeasterly over northwest Australia, compared to northwesterly in the climatology. This is further evidence to support the results from the case study, which suggests that the bore-like waves form under low-level southeasterly synoptic-scale flow.

Prior to this study, Smith (1986) provided the only well-documented study of wave-cloud lines over northwest Australia. The Smith (1986) study had a similar structure to the cloud lines in the first case study of this paper. Smith (1986) suggested that the disturbance was caused by the collision of the onshore sea breeze with a southeasterly offshore flow. The main difference between this case and the case in the present study is that a region of thunderstorms were present inland of the coast during the Smith (1986) case. It appeared that the southeasterly offshore flow was produced by a gust front associated with the region of convection, rather than by the synoptic-scale flow. This was not the case for most of the bore-like wave-clouds that were identified from the satellite imagery; almost all the identified occurrences of bore-like clouds occurred on days when significant convection was absent from northwest Australia. It could be that the gust front simply acted to reinforce the synoptic-scale flow in the Smith (1986) case, i.e. the wave-cloud would have formed even if the storm was not present.

The second case study focused on convectively-generated waves. The satellite imagery associated with this case shows two cloud lines, which are much more circular in shape than the bore-like wave clouds in the first case study. The waves are seen to propagate away from two convective regions that are present close to the northwest coast of Australia. The model simulation of this case successfully reproduces regions of deep convection adjacent to the coast and waves that propagate outwards from the convection centre. The waves appear to be n=2 wave-front type waves, which propagate along the entire depth of the troposphere and appear to be produced during a period of significant updrafts in the convective system. These waves are very different in structure to the bore-like waves discussed in the first part of this study; they propagate along the entire depth of the troposphere, as opposed to a specific layer and they are much more circular in shape compared to the more linear cloud lines associated with the bore-like waves.

Unlike the observations, cloud is not associated with the convectively-generated waves in the model simulations. This could be because the amplitude of the waves is not large enough in the model to lift air above its condensation level. The location of the waves in the model simulations also does not agree exactly with the locations of the waves in the satellite imagery. It is perhaps not surprising that the bore-like waves, produced by a sea breeze mechanism, are better resolved by the model than waves that are produced by convective processes.

Acknowledgements

The authors would like to thank the Royal Meteorological Society for providing travel funding via the Rupert Ford Award for CEB to visit Monash University. CEB is also funded by NERC grant NE/G018499/1. We are grateful for the help of Grenville Lister and William McGinity from the National Centre for Atmospheric Science (NCAS) model support helpdesk for providing model analyses and assistance with model issues. We would like to thank the Dundee Satellite Receiving Station for providing satellite imagery and the European Centre for Medium-Range Weather Forecasts (ECMWF) and the British Atmospheric Data Centre (BADC) for providing access to the

ERA-Interim data set.

Appendix

Consider an atmosphere in which the wind is constant with height and choose a coordinate frame moving with the wind. Assume also that the atmosphere comprises three layers; the lowest layer, Layer 1, is neutrally stratified, meaning the Brunt-Vaisala frequency, N_1, is zero. It is bounded above by the interface with the middle layer at $z = H$ and bounded below by a rigid surface at $z = 0$. The middle layer, Layer 2, has depth h and a Brunt-Vaisala frequency, N_2, which is positive and constant. The top layer, Layer 3, is also stratified; it begins at $z = H + h$, the interface between Layers 2 and 3, and is unbounded above. The variables discussed above are illustrated in Figure 13b.

The Taylor-Goldstein equation describes the vertical structure $\hat{\psi}_j(z)$ of small amplitude two-dimensional plane waves of the form $\psi = \hat{\psi}_j(z)e^{ik(x-ct)}$:

$$\frac{d^2\hat{\psi}_j}{dz^2} + m_j^2\hat{\psi}_j = 0 \qquad \text{(A1)}$$

where j is the layer (1,2 or 3), $m_j^2 = N_j^2/c^2 - k^2$ is the vertical wavenumber, k is the horizontal wavenumber and c is the phase speed.

Equation A1 is solved in each layer with $\hat{\psi}_3$ bounded as $z \to \infty$. These solutions are matched at the two interfaces using the kinematic and dynamic conditions that $\hat{\psi}_j$ and $d\hat{\psi}_j/dz$ are continuous at $z = H$ and $z = H + h$. Whereupon, the solution is:

$$\hat{\psi}(z) = Ae^{-m_3(H+h)} \begin{cases} 1 & z > H+h \\ \cos\left[m_2(z-H-h)\right] - \dfrac{m_3}{m_2}\sin\left[m_2(z-H-h)\right] & H \geq z \geq H+h \\ \left(1-m_3(z-H)\right)\cos\left(m_2 h\right) - \left(\dfrac{m_3}{m_2} + m_2(z-H)\right)\sin\left(m_2 h\right) & 0 > z \geq H \end{cases}$$

where A is an arbitrary constant. To satisfy the lower boundary condition, $\hat{\psi} = 0$ at $z = 0$,

$$\left(1+m_3 H\right)\cos\left(m_2 h\right) - \left(\frac{m_3}{m_2} - m_2 H\right)\sin\left(m_2 h\right) = 0 \cdot \qquad \text{(A2)}$$

Equation (A2) is solved numerically for *c* given *H*, *h*, N_2 and N_3.

References

Arnup SJ, Reeder MJ. 2007. The diurnal and seasonal variation of the northern Australian dryline. *Mon. Wea. Rev.* **135**: 2995-3008.

Atkinson, RW. 1981. *Meso-scale Atmospheric Circulations*, Academic Press, p495.

Birch CE, Parker DJ, O'Leary A, Marsham JH, Taylor CM, Harris P, Lister G. 2012. The impact of soil moisture and convectively-generated waves on the initiation of a West African mesoscale convective system. Submitted to *Quart. J. Roy. Meteor. Soc.*

Bretherton CS, Smolarkiewicz PK. 1989. Gravity waves, compensating subsidence and detrainment around cumulus clouds. *J. Atmos. Sci*. **46**: 740–759.

Christie DR. 1992. The morning glory of the Gulf of Carpentaria: a paradigm for non-linear waves in the lower atmosphere. *Aust. Met. Mag.* **41**: 21-60.

Christie DR, Muirhead KJ. 1983. Solitary waves: A hazard to aircraft operating at low altitudes. *Austr. Met. Mag*. **31**: 97-109.

Clarke RH, 1972. The morning glory: an atmospheric hydraulic jump. *J. Appl. Met.* **11**: 304-311.

Clarke RH, Smith RK, Reid DG. 1981. The Morning Glory of the Gulf of Carpentaria: An atmospheric undular bore. *Mon. Wea. Rev.* **109**: 1726-1750.

Davies T, Cullen MJP, Malcolm AJ, Mawson MH, Staniforth A, White AA, Wood S. 2005. A new dynamical core for the Met Office's global and regional modelling of the atmosphere. *Quart. J. Roy. Meteor. Soc.* **131**: 1759–1782.

Davis WM, Schultz LG, Ward RD. 1889. An investigation of the sea-breeze. *New. Engl. Meteor. Soc. Obser.* **21**: 214-264.

Dee DP, Uppala SM, Simmons AJ, Berrisford P, Poli P, Kobayashi S, Andrae U, Balmaseda MA, Balsamo G, Bauer P, Bechtold P, Beljaars ACM, van de Berg L, Bidlot J, Bormann N, Delsol C, Dragani R, Fuentes M, Geer AJ, Maimberger L, Healy SB, Hersbach H, Hólm EV, Isaksen L, Kållberg P, Köhler M, Matricardi M, McNally AP, Monge-Sanz BM, Morcrette J-J, Park B-K, Peubey C, de Rosnay P, Tavolato C, Thépaut J-N, Vitart F. 2011. The ERA-Interim reanalysis: configuration and performance of the data assimilation system. *Quart. J. Roy. Meteor. Soc.* **137**: 553–597.

Deslandes R, Reeder MJ, Mills G. 1999. Synoptic analyses of a subtropical cold front observed during the 1991 Central Australian Fronts Experiment. *Aust. Met. Mag.* **48**: 87-110.

Drosdowsky W. 1996 Variability of the Australian summer monsoon at Darwin: 1957-1992. *J. Climate*. **9**: 85-96.

Essery RLH, Best MJ, Cox PM. 2001. MOSES 2.2 technical documentation. Technical report, Met Office. 14 August 2001.

Goler RA, Reeder MJ. 2004, The generation of the morning glory. *J. Atmos. Sci.* **61**: 1360-1376.

Gregory D, Rowntree PR. 1990. A mass flux convection scheme with representation of cloud ensemble characteristics and stability-dependent closure. *Mon. Wea. Rev.* **118**: 1483–1506.

Haase SP, Smith RK, 1984. Morning glory wave-clouds in Oklahoma: A case study. *Mon. Wea. Rev.* **112**: 2078-2089.

Haase SP, Smith RK. 1988. The numerical simulation of atmospheric gravity currents, Part II. Environments with stable layers. *Geophys. Astrophys. Fluid Dyn*. **46**: 35-51.

Kingwell J. 1984. Observations of a quasi-circular squall line off north-west Australia. *Weather*. **39**: 343-346.

Koch SE, Zhang F, Kaplan ML, Lin Y-L, Weglarz R, Trexler CM. 2000. Part III: The role of a mountain-plains solenoid in the generation of the second wave episode. *Mon. Wea. Rev*. **129**: 909-933.Koch SE, Feltz W, Fabry F, Pagowski M, Geerts B, Bedka KM, Miller DO, Wilson JW. 2008. Turbulent mixing processes in atmospheric bores and solitary waves deduced from profiling systems and numerical simulation. *Mon. Wea. Rev*. **136**: 1373–1400.

Lac C, Lafore JP, Redelsperger JL. 2002. Role of gravity waves in triggering deep convection during TOGA COARE. *J. Atmos. Sci*. **59**: 1293–1316.

Lane TP, Reeder MJ. 2001. Convectively generated gravity waves and their effect on the cloud environment. *J. Atmos. Sci*. **58**: 2427–2440.

Lane TP, Zhang F. 2011. Coupling between gravity waves and tropical convection at mesoscales. *J. Atmos. Sci*. **68**: 2582-2597.Lock AP, Brown AR, Bush MR, Martin GM, Smith RNB. 2000. A new boundary layer mixing scheme. Part I: Scheme description and single-column model tests. *Mon. Wea. Rev.* **128**: 3187–3199.

Neal AB, Butterworth IJ. 1973. The recurring cloud line in the Gulf of Carpentaria. *Working Paper*

163. Bur. Met., Australia.

Mapes BE. 1993. Gregarious tropical convection. *J. Atmos. Sci.* **50**: 2026-2037.

Marsham JH, Parker DJ. 2006. Secondary initiation of multiple bands of cumulonimbus over southern Britain. II: Dynamics of secondary initiation. *Quart. J. Roy. Meteor. Soc.* **132**: 1053–1072.

Pope M, Jakob C, Reeder MJ. 2008. Convective systems of the North Australian Monsoon. *J. Climate*, **21**: 5091-5112.

Qian T, Epifanio CC, Zhang F. 2012: Topographic effects on the tropical land and sea breeze. *J. Atmos. Sci*, **69**: 130-149.

Reeder MJ, Smith RK. 1998. Mesoscale meteorology. *Meteorol. Mono.* **27**: 201-241.

Reeder MJ, Smith RK, Taylor T, Low DJ, Arnup SJ, Muir L, Thomsen G. 2012. Diurnally-forced convergence lines in the Australian Tropics. Submitted to *Quart. J. Roy. Meteor. Soc.*

Schmidt CW, Goler RA. 2010. Nonlinear waves ahead of fronts in the Great Australian Bight. *Mon. Wea. Rev.* **138**: 3474-3497.

Scorer RS. 1997. *Dynamics of Meteorology and Climate*. Praxis Publishing Ltd, Chichester, England; pp 155-161.

Smith RK, Crook N, Roff R. 1982. The morning glory: an extraordinary undular bore. *Quart. J. Roy. Meteor. Soc.* **108**: 937-956.

Smith RK. 1986. Evening glory wave-cloud lines in northwestern Australia. *Aust. Met. Mag.* **34**: 27-33.

Smith RK, Reeder MJ, Tapper NJ, Christie, DR. 1995. Central Australian Cold Fronts. *Mon. Wea.*

Rev. **123**: 16-38.

Thomsen GL, Reeder MJ, Smith RK. 2009. The diurnal evolution of cold fronts in the Australian subtropics. *Quart. J. Roy. Meteor. Soc.* **135**: 395–411.

Wilson DR, Ballard SP. 1999. A microphysically based precipitation scheme for the U.K. Meteorological Office Unified Model. *Quart. J. Roy. Meteor. Soc.* **125**: 1607–1636.

Zhang F, Koch SE. 2000: Numerical simulations of a gravity wave event over CCOPE. Part II: Waves generated by an orographic density current. *Mon. Wea. Rev*. **128**: 2777-2796.

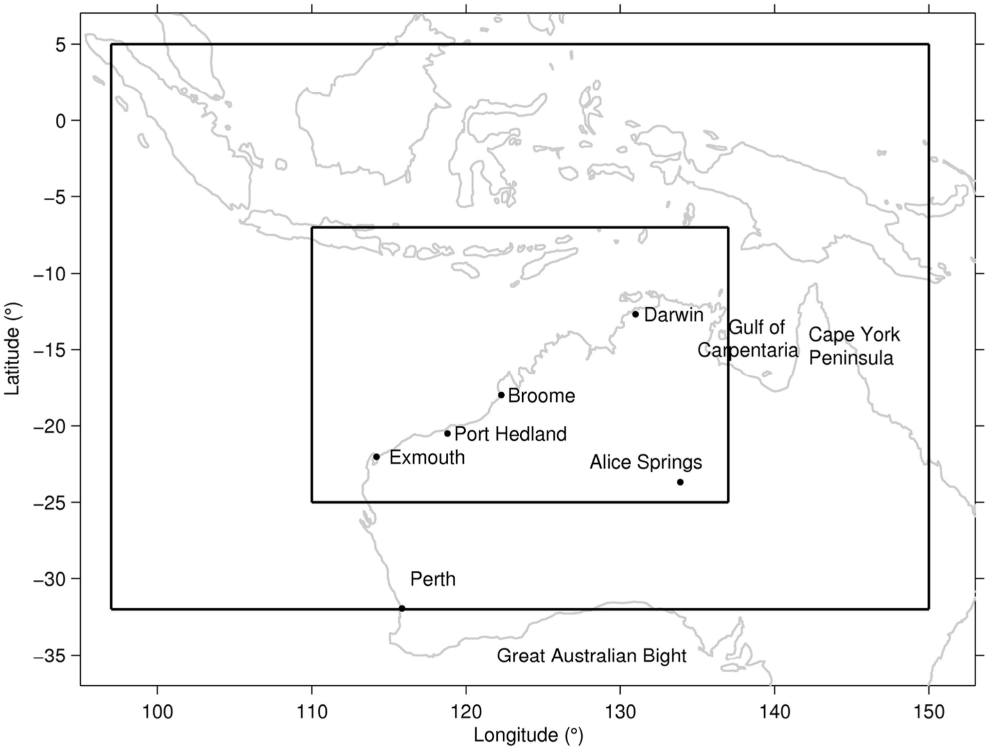

Figure 1 12 and 4-km model nest domains and the locations of places mentioned in the text.
136x103mm (300 x 300 DPI)

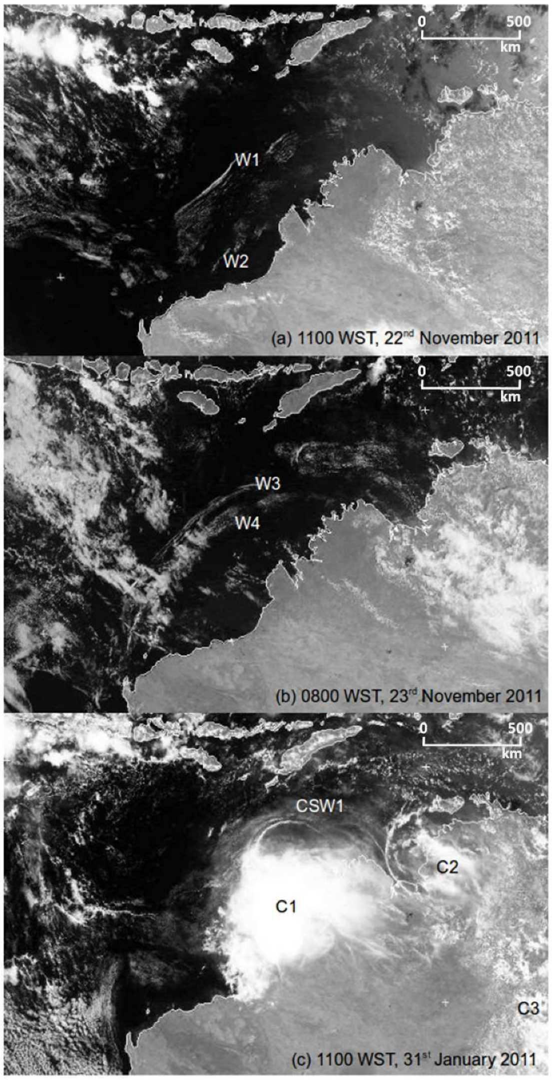

Figure 2 Visible satellite imagery at (a) 1100 WST 22nd November 2011, (b) 0800 WST 23rd November 2011 and (c) 1100 WST 31st January 2011 from the MTSAT.
265x375mm (300 x 300 DPI)

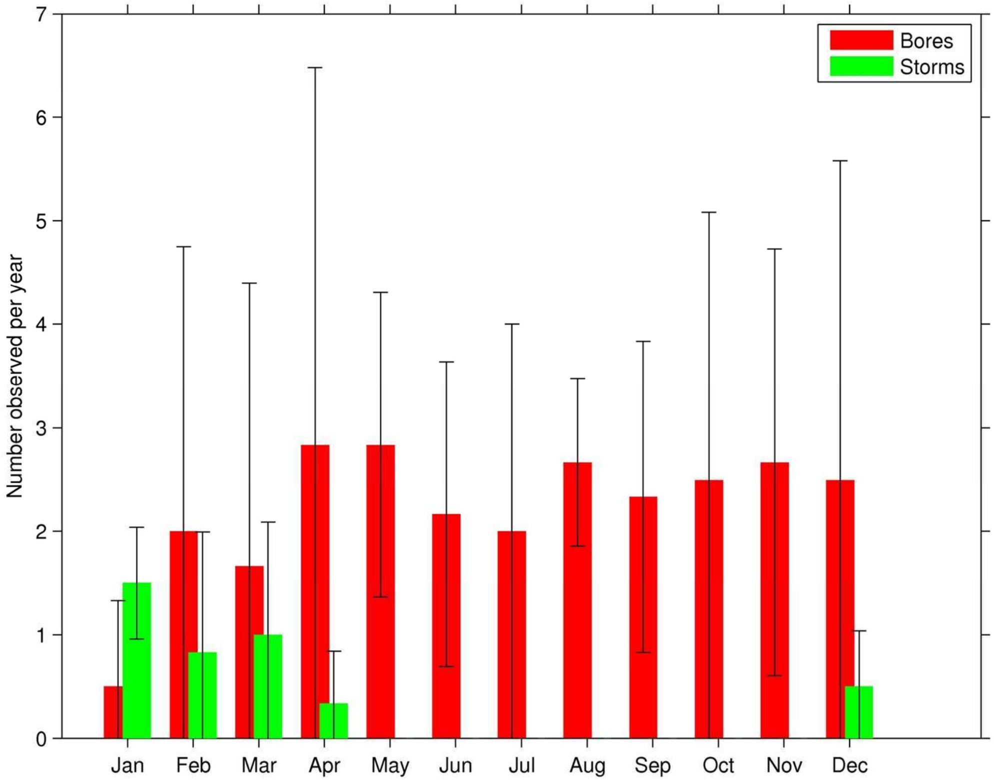

Figure 3 Number of bore-like cloud structures (red) and wave clouds from convective storms (green) identified per year by visible satellite images (MTSAT), 2006-2011. The bars mark plus/minus the standard deviation of the monthly totals for each year.
135x106mm (300 x 300 DPI)

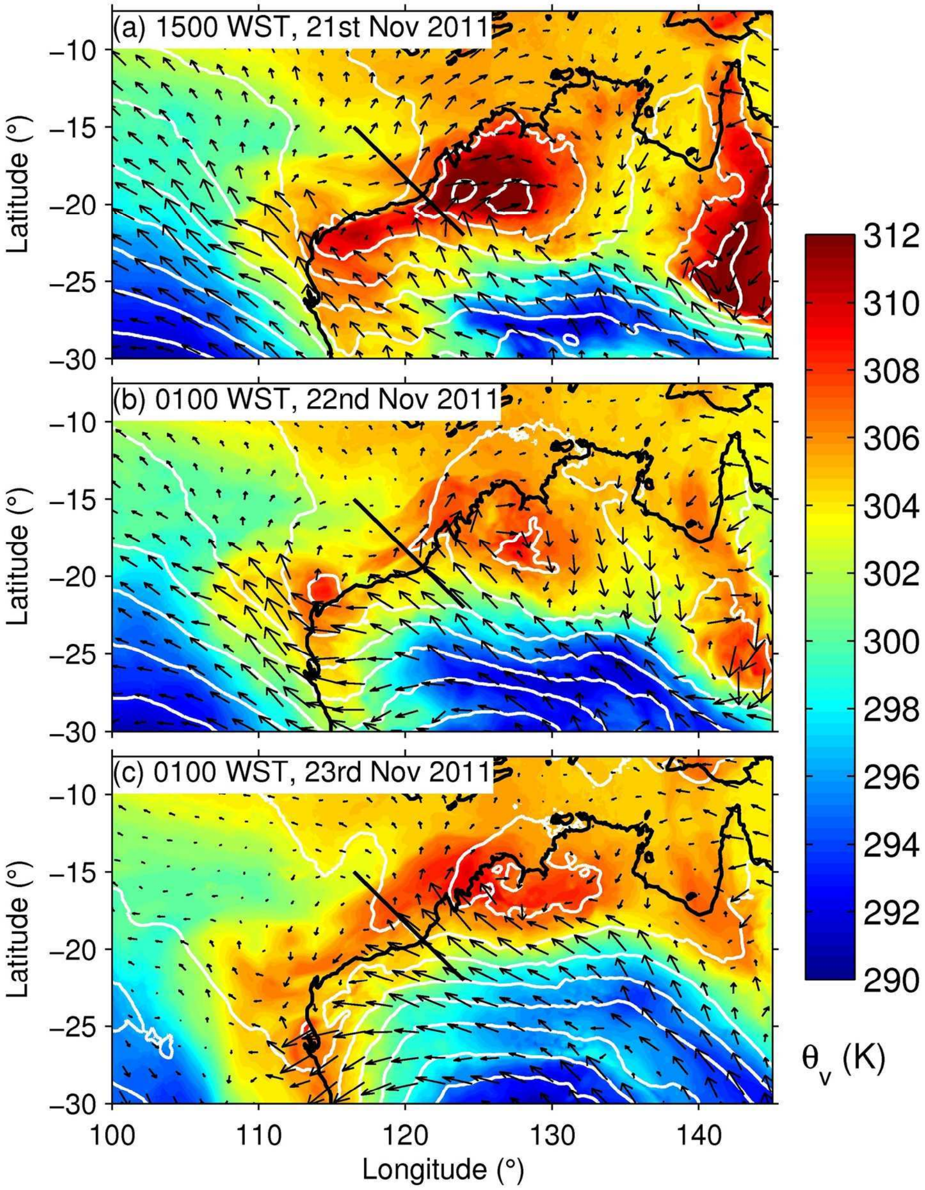

Figure 4 925h Pa θ_v (shading), 925 hPa winds (vectors) and MSLP pressure (white contours) from the 12-km model nest. The solid, diagonal black line marks the diagonal transect used in Figures 7-11.
147x187mm (300 x 300 DPI)

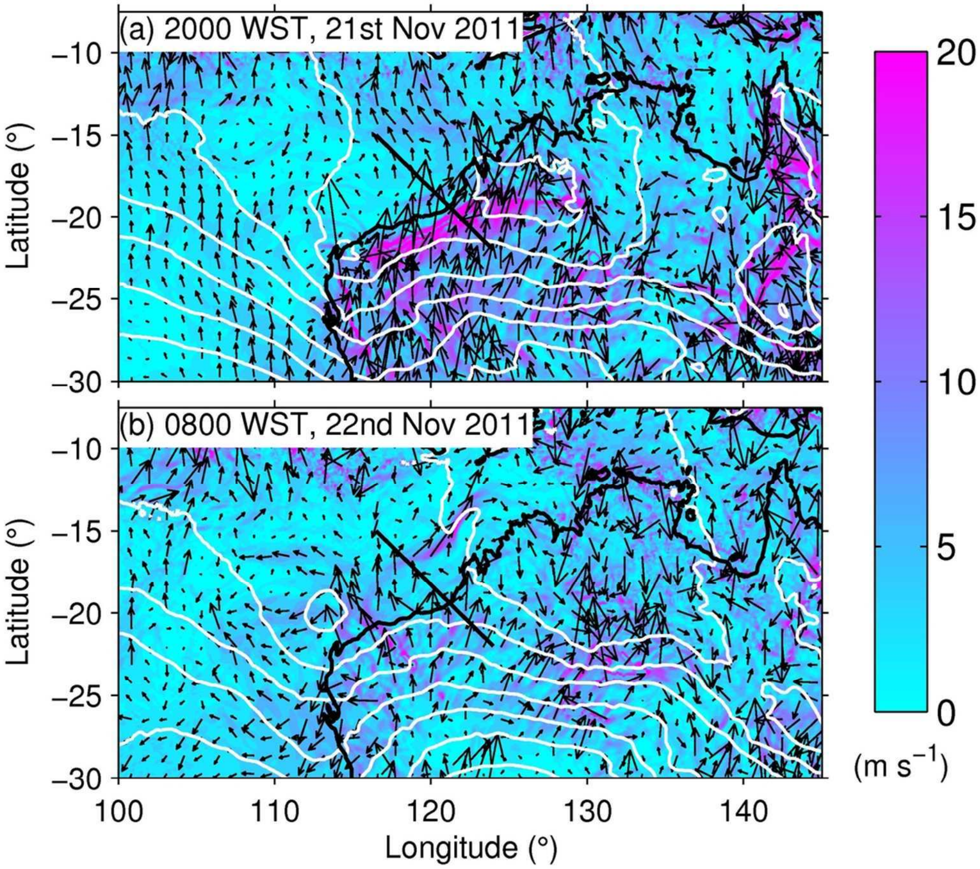

Figure 5 925 hPa ageostrophic wind component (shading and vectors) and MSLP (white contours) from the 12-km model nest. The solid, diagonal black line marks the diagonal transect used in Figures 7-11.
101x89mm (300 x 300 DPI)

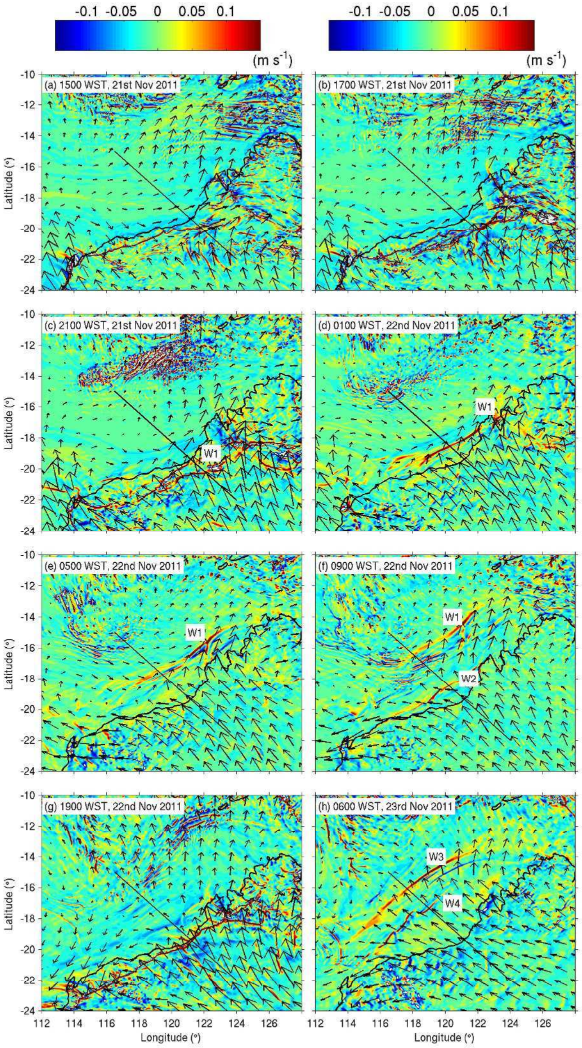

Figure 6 925 hPa vertical velocity from the 4-km model nest. The solid, diagonal black line marks the diagonal transect used in Figures 7-11.
355x622mm (300 x 300 DPI)

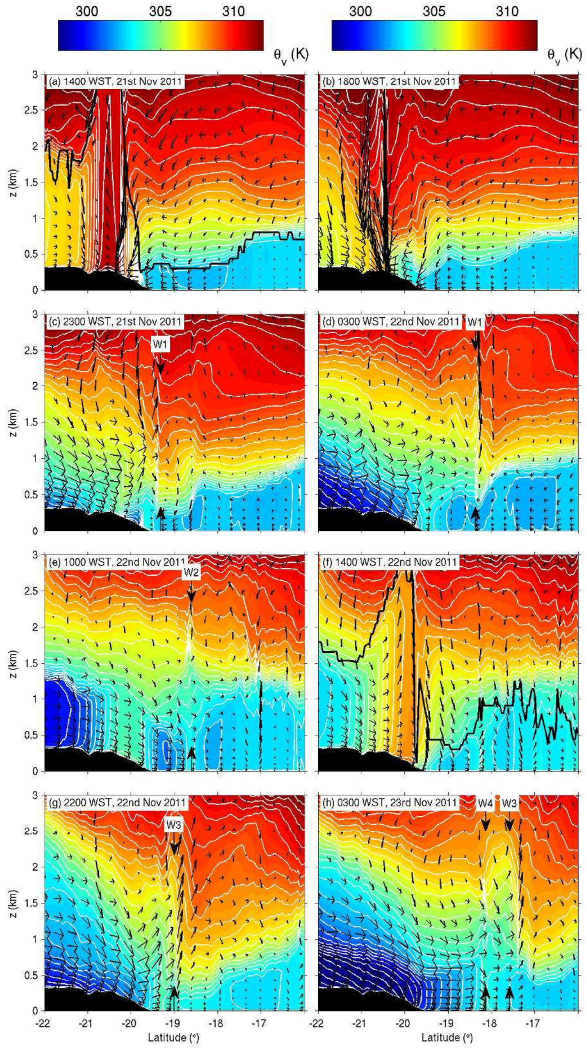

Figure 7 Cross section of θ_v (shading and white contours) and along-transect and vertical wind vectors along the diagonal section from the 4-km nest. The thick black contour in (a) and (f) shows the model boundary-layer depth diagnostic.
355x622mm (300 x 300 DPI)

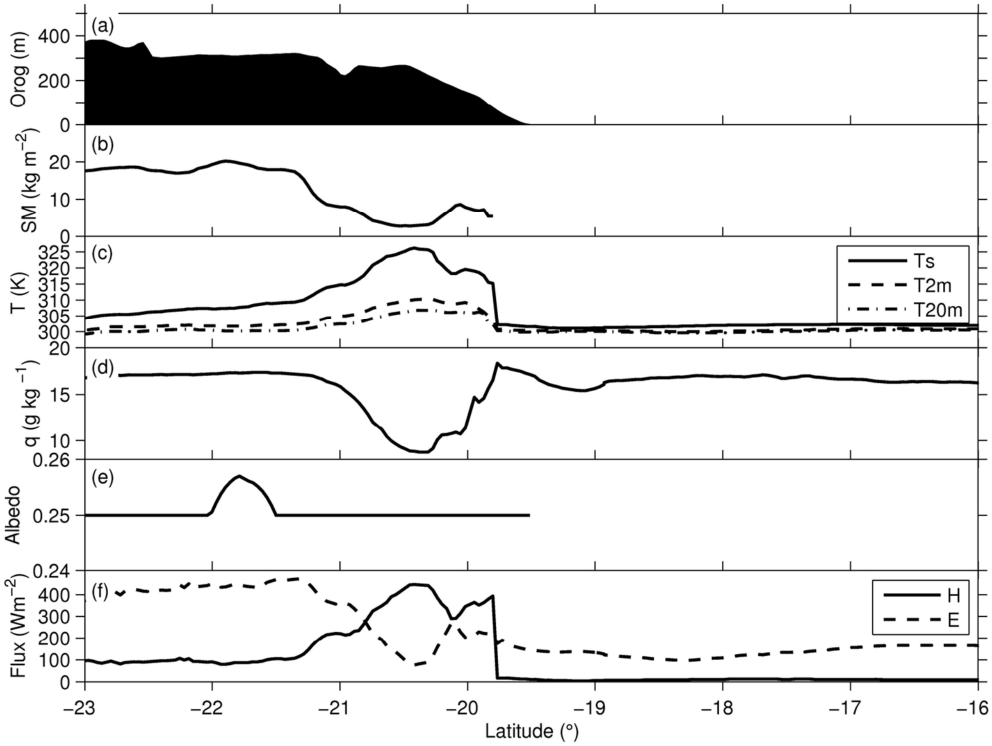

Figure 8 Surface variables from the 4-km model nest along the diagonal cross section at 1100 WST, 21st November 2011. (a) Orography height, (b) soil moisture, (c) surface temperature, T_s, 2 m air temperature, T_{2m}, and 20 m air temperature, T_{20m}, (d) 2 m specific humidity, (e) albedo and (f) sensible, H and latent, E heat fluxes.

136x102mm (300 x 300 DPI)

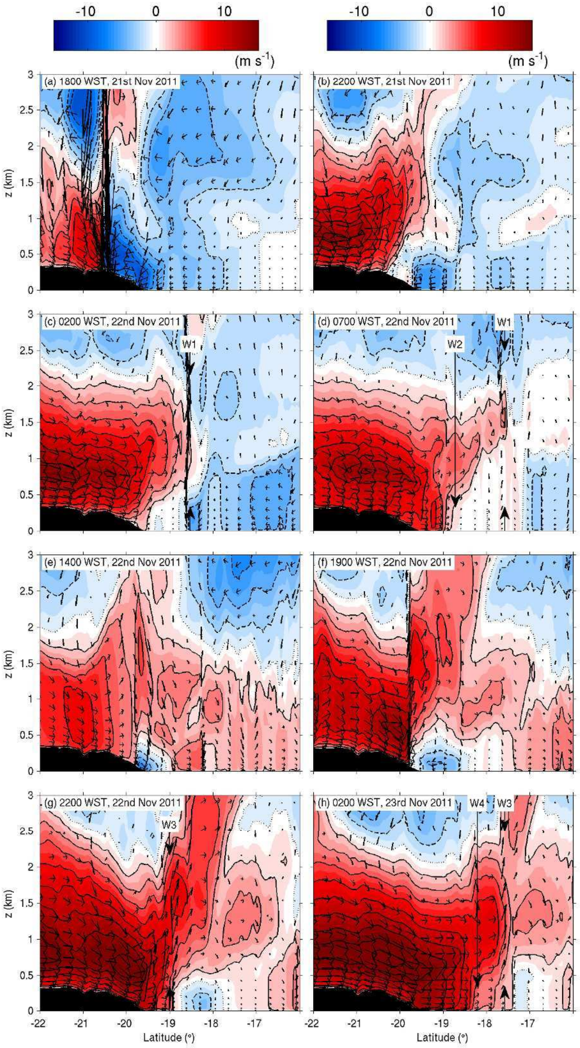

Figure 9 Along-transect wind speed (shading and contours) and along-transect and vertical wind vectors from the 4-km nest.
355x622mm (300 x 300 DPI)

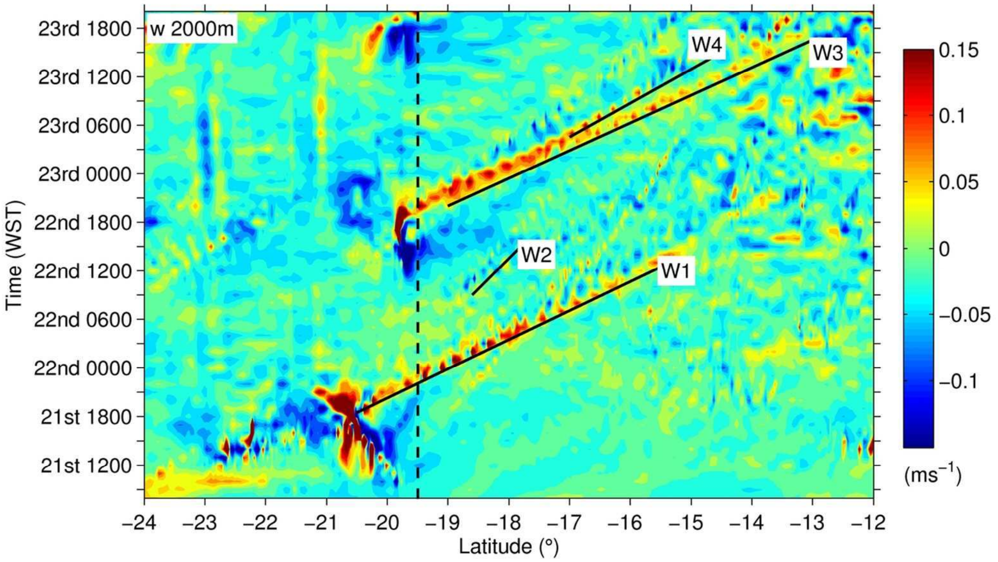

Figure 10 Hovmöller plot of vertical velocity at 2000 m above mean sea level from the 4-km nest. The vertical dashed line marks the location of the coast.
120x71mm (300 x 300 DPI)

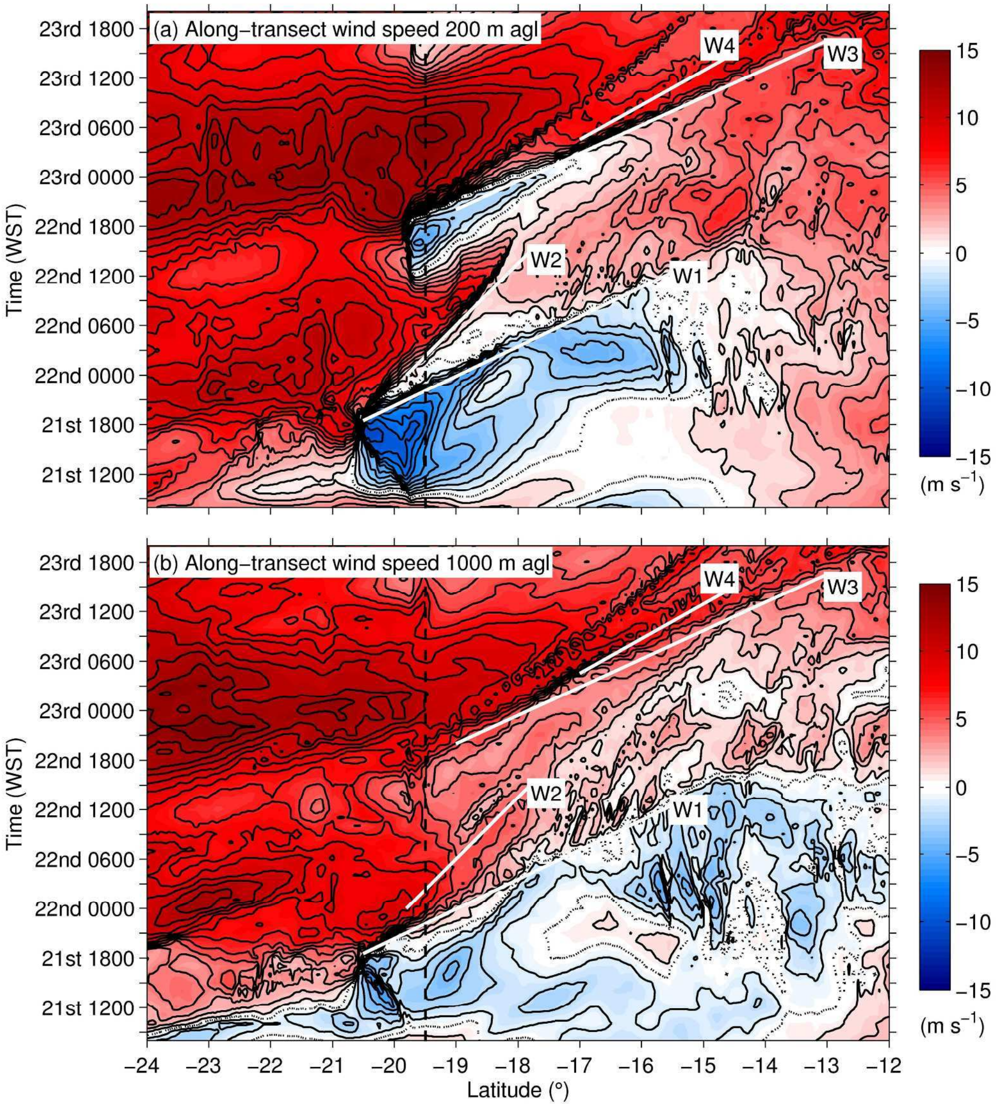

Figure 11 Hovmöller plots of (a) along-transect wind speed and (b) θ_v at 200 m above ground level from the 4-km nest. The vertical dashed lines mark the location of the coast.
226x257mm (300 x 300 DPI)

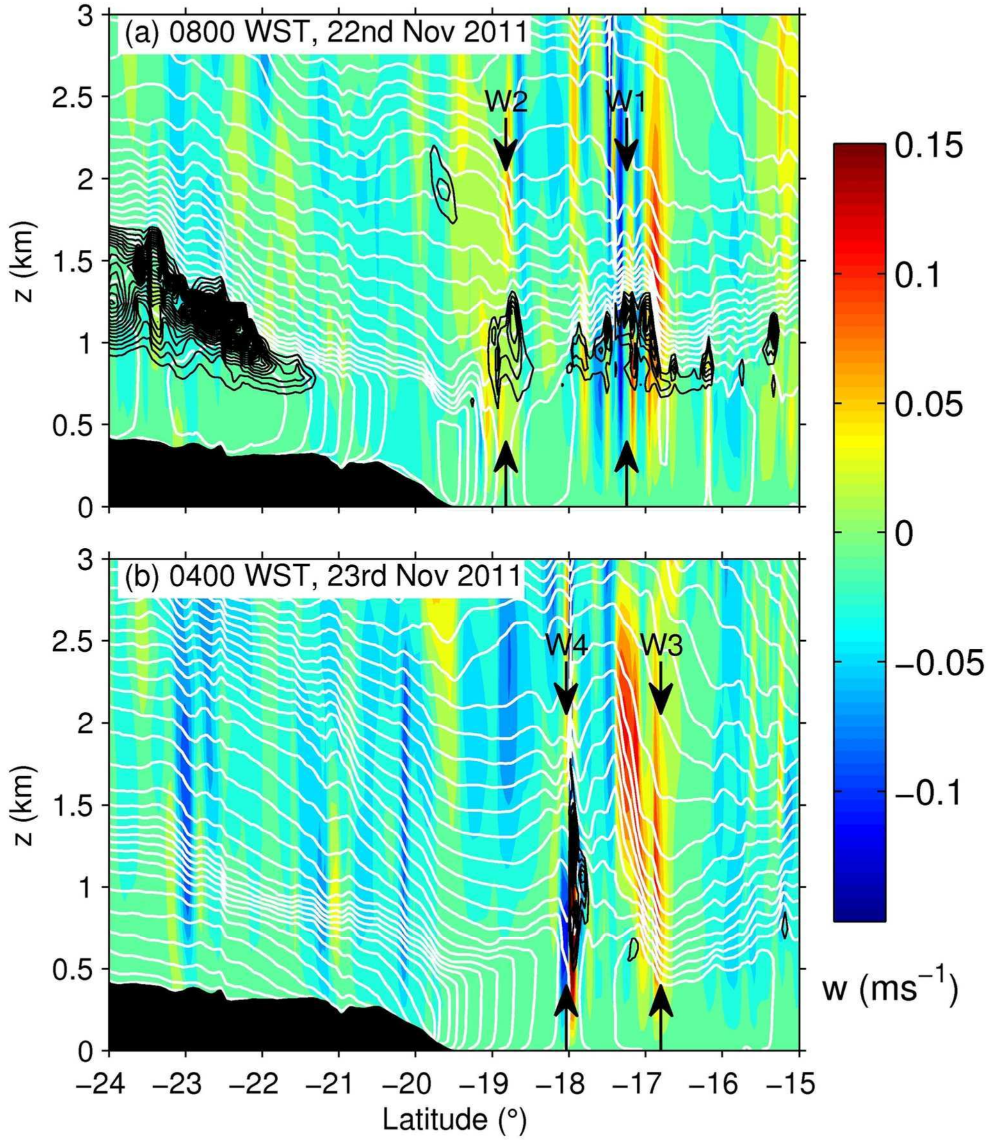

Figure 12 Cross section of vertical velocity (shading), θ_v (white contours) and frozen and liquid cloud water (black contours) from the 4-km model nest.
136x158mm (300 x 300 DPI)

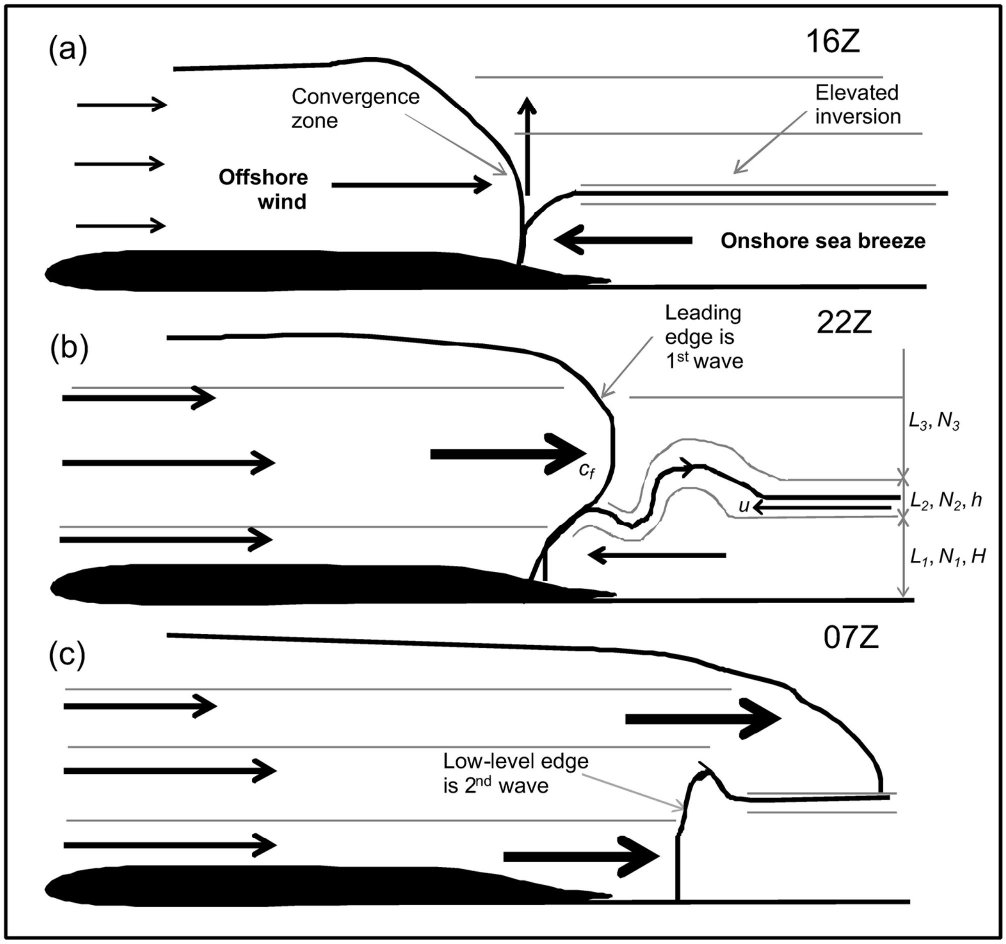

Figure 13 Schematic illustrating the wave formation mechanisms
162x151mm (300 x 300 DPI)

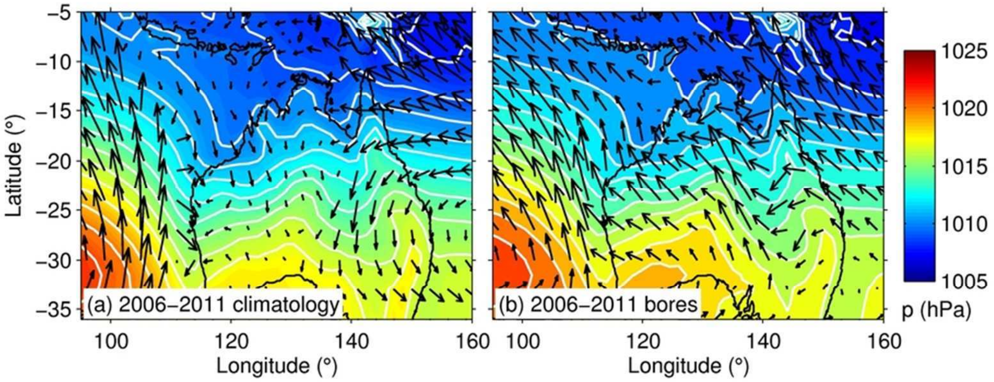

Figure 14 MSLP and 950 hPa wind vectors at 1800 UTC (0200 WST), (a) averaged over 2006-2011 and (b) averaged over days when a bore-like wave was observed in the satellite imagery.
77x30mm (300 x 300 DPI)

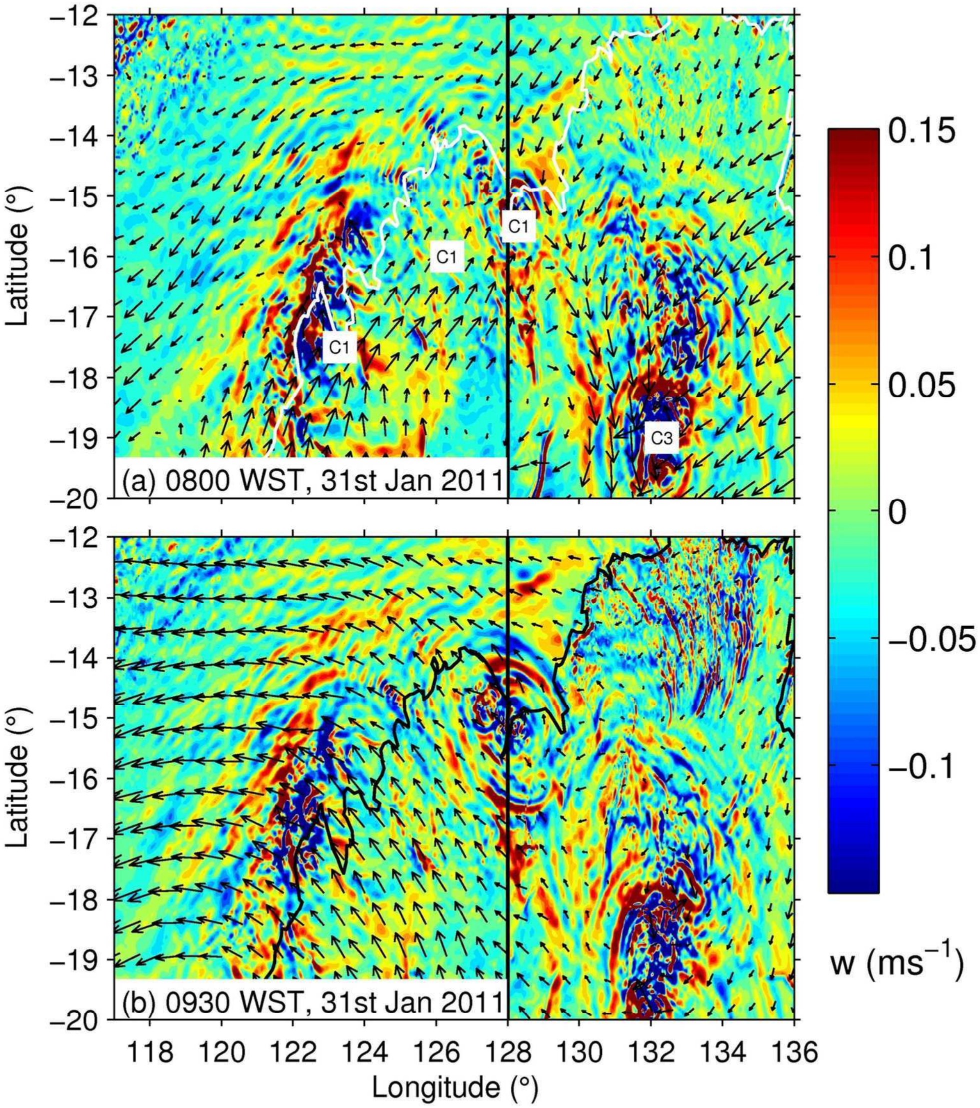

Figure 15 (a) 850 hPa vertical velocity (shading) and 850 hPa horizontal wind vectors and (b) 850 hPa vertical velocity (shading) and 600 hPa horizontal wind vectors at 0800 and 0930 WST from the 4-km nest. The vertical black line is the section used in Figures 14 and 15.
135x152mm (300 x 300 DPI)

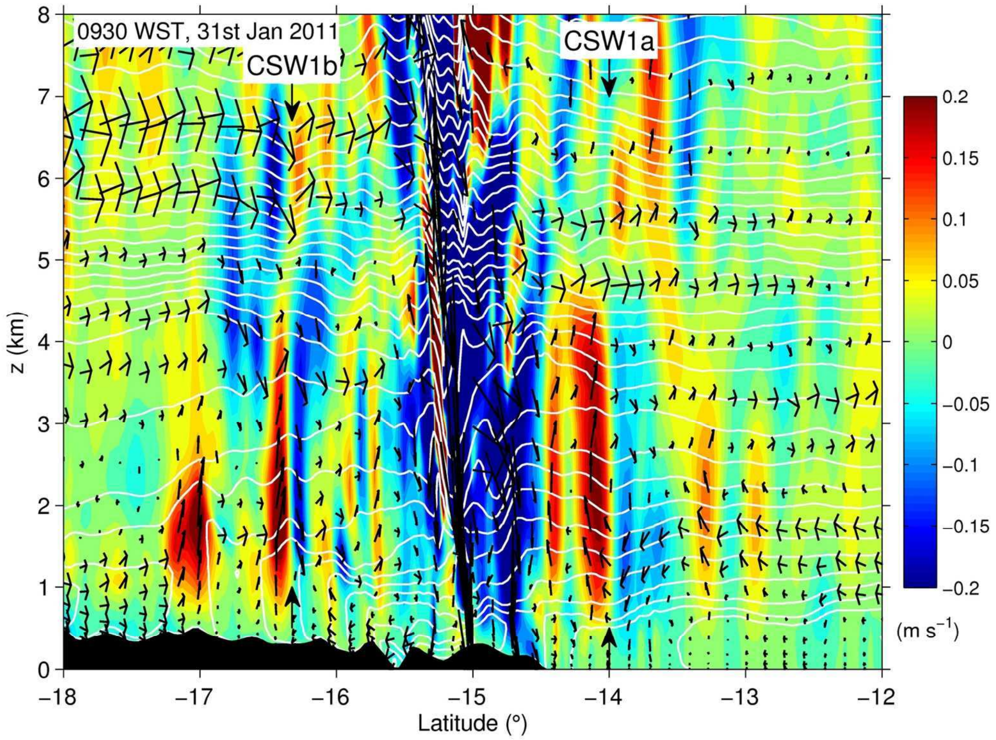

Figure 16 Vertical velocity (shading) and θ_v (white contours) along 128E at 0930 WST from the 4-km nest. The waves are marked by the arrows.
139x104mm (300 x 300 DPI)

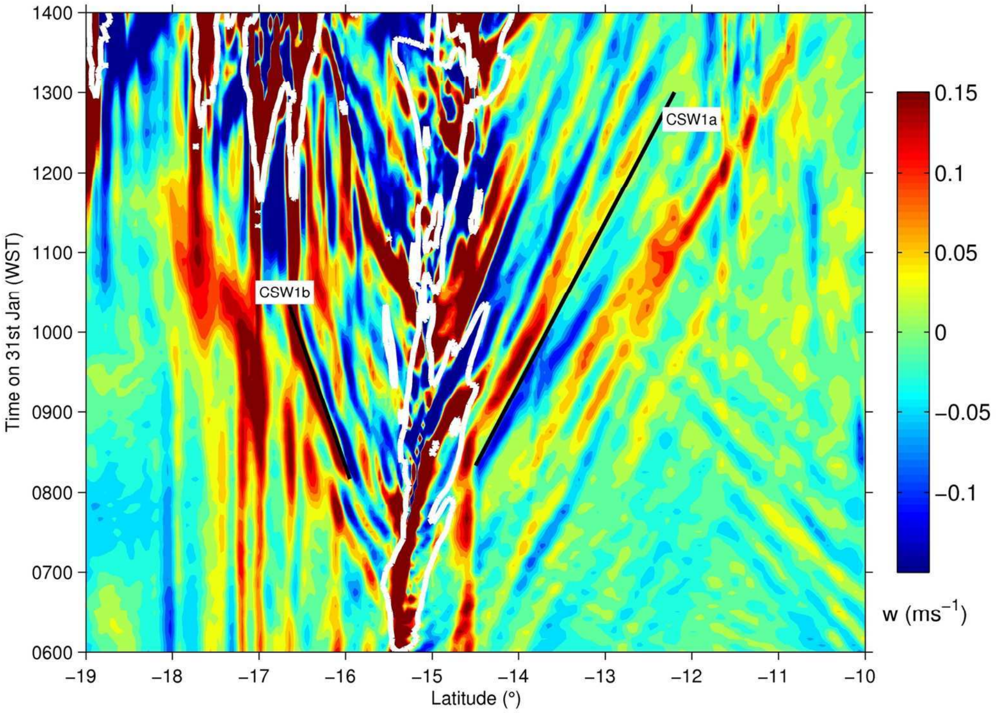

Figure 17 Hovmöller of 850 hPa vertical velocity (shading) and 70% medium cloud fraction (white contours) along 128E from the 4-km nest. The solid black lines mark the propagation of the CSW1 and CSW2 waves.
141x104mm (300 x 300 DPI)